Coupling channel effects on K^-p correlation function using a cut off regularization

Author: Erick Einar Garcia Gonzales
Facultat de Física, Universitat de Barcelona, Diagonal 645, 08028 Barcelona, Spain.

Advisor: Volodymyr Magas
(Dated: January 13, 2024)

Abstract: Studying the interaction between K^- and protons in the $S = -1$ sector must be done considering all possible contributions coming from other channels. In this sense, this work studies the effects each of these channels have on the K^-p correlation function. We also try to extract information about the contributions of the interaction potential which was obtained from a Chiral Unitary Approach. Theoretical results will be compared with available data from Alice Collaboration at CERN.

I. INTRODUCTION

Two particle correlations obtained from heavy ion collisions was extensively used to study the space-time structure of the particle emitting source [1, 2]. Nevertheless, correlations can also be used to study and extract information about the interaction between particles [3].

Quantum Chromodynamics (QCD) is the theory that explains interactions between quarks and gluons, however, it is not suitable to describe low energy hadron interactions. For this reason, effective theories that preserve the symmetries from QCD are used to explain low energy dynamics. The effective theory that explains appropriately the meson-meson and meson-baryon interactions is the SU(3) Chiral Unitary Approach (ChUA) [4–6], which applies unitarization via coupled channels. In the context of meson-baryon interaction with strangeness $S = -1$ the theory couples the pseudoscalar meson octet (π, K, η) and the baryon octet (N, Λ, Σ, Ξ) producing, thus, 10 possible channels: K^-p, $\bar{K}^0n$, $\pi^0\Lambda$, $\pi\Sigma$, $\eta\Lambda$, $\eta\Sigma^0$, $K^+\Xi^-$, $K^0\Xi^0$.

The effective Lagrangian in ChUA reads

$$\mathcal{L} = \mathcal{L}_\phi + \mathcal{L}_{\phi B}\,,$$

where $\mathcal{L}_\phi$ is exclusively mesonic, so it can be omitted. The second term takes into consideration the meson-baryon interaction and it will be expanded to next-to-leading order (NLO) [4],

$$\mathcal{L}_{\phi B} = \mathcal{L}^{(1)}_{\phi B} + \mathcal{L}^{(2)}_{\phi B}. \tag{1}$$

Fig. 1 shows the Feynman diagrams for all the meson-baryon interactions terms making up the interaction potential. The Weinberg-Tomaza term, V^{WT}, corresponds to diagram (i), diagrams (ii) and (iii) are, respectively, direct Born (V^{DB}) and crossed Born (V^{CB}) terms; all these contributions come from the first order term at Eq. (1). And, finally, the diagram (iv) is the representation of the interaction to next to leading order, V^{NLO}.

Thus, the interaction potential up to NLO will be made up of the following terms:

$$V = V^{WT} + V^{DB} + V^{CB} + V^{NLO}. \tag{2}$$

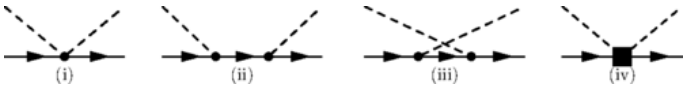

FIG. 1: Feyman diagrams of the interaction terms forming the interaction potential obtained from ChUA to NLO. (i) Weinberg-Tomazawa term. (ii) Direct Born. (iii) Crossed Born term. (iv) NLO term.

The model of Ref. [4] considers only S-wave meson-baryon interaction, and its parameters are obtained fitting the model to available cross sections of the $K^-p \to K^-p, \bar{K}^0n, \pi^0\Lambda, \pi\Sigma, \eta\Lambda, \eta\Sigma^0, K^+\Xi^-, K^0\Xi^0$ reactions. In the following we will use this model [4] for our calculations.

II. LIPPMANN-SCHWINGER EQUATION

All the information about a scattering process of particles is contained in the scattering amplitude or T matrix. This matrix can be obtained from the interaction potential solving the Lippmann-Schwinger equation [6, 7]:

$$T_{ij}(\sqrt{s}, \vec{k}_i, \vec{k}_j) = V_{ij}(\sqrt{s}, \vec{k}_i, \vec{k}_j) + \sum_k i \int \frac{d^4q_k}{(2\pi)^4} V_{ik}(\sqrt{s}, \vec{k}_i, q_k)\hat{G}_k(\sqrt{s}, q_k)T_{kj}(\sqrt{s}, q_k, \vec{k}_j). \tag{3}$$

In the expression above, $\hat{G}$ is the Green propagator, i is the index for the initial meson-baryon channel, j is the index for the final channel, q_k is the total four momentum of the virtual particles, V the interaction potential (Eq. (2)), $\vec{k}_i$ the relative momentum of the particles in channel i and $\sqrt{s}$ the energy of the system.

Under certain conditions we, considering the on-shell interaction ($q_k^2 = m_k^2$), can factorize the integral of Eq. (3) and reduce it to a set of algebraic equations [6]:

$$T_{ij}(\sqrt{s}) = V_{ij}(\sqrt{s}) + \sum_k V_{ik}(\sqrt{s})G_k(\sqrt{s})T_{kj}(\sqrt{s})\,. \tag{4}$$

In matrix form it can be solved as follows

$$T = V + VGT = (1 - VG)^{-1}V\,, \tag{5}$$

where G is the loop function. For meson-barion interaction, G is defined as

$$G_k(\sqrt{s}) = i \int \frac{d^4q_k}{(2\pi)^4} \frac{2M_k}{(P-q_k)^2 - M_k^2 + i\epsilon} \frac{1}{q_k^2 - m_k^2 + i\epsilon}, \tag{6}$$

with M_k and m_k the baryon and meson masses from channel k and P the total four-momentum of the system ($P = (\sqrt{s}, 0)$ in the center of mass frame). Integrating over q_k^0, we arrive to the following equation

$$G_k(\sqrt{s}) = \int_0^{q_{max}} \frac{q^2 dq}{4\pi^2} \frac{2M_k}{E_{1k}E_{2k}} \frac{E_{1k}+E_{2k}}{s-(E_{1k}+E_{2k})^2+i\epsilon}, \tag{7}$$

where E_{1k} and E_{2k} are the energies of the baryon and meson. The loop integral at Eq. (7) diverges, therefore it has to be regularized in some way, typically via dimensional regularization or cutt off methods. In [8] there is an analytical expression for the loop function obtained using a cut off method; we shall call that expression $G^{CR}(\sqrt{s}, q_{max})$ (Eq. (A1) in Ref. [8]).

III. CORRELATION FUNCTION TREATMENT

The momentum correlation of two particles is given by the Koonin-Pratt formula [3, 9]

$$C(\vec{p}_1, \vec{p}_2) = \frac{\int d^4x_1 d^4x_2 S_1(x_1, \vec{p}_1) S_2(x_2, \vec{p}_2) \left|\Psi^{(-)}(\vec{r}, \vec{k})\right|}{\int d^4x_1 d^4x_2 S_1(x_1, \vec{p}_1) S_2(x_2, \vec{p}_2)}, \tag{8}$$

where S_i is the single particle source function, $\vec{p}_i$ the momentum of the particle i, $\Psi^{(-)}$ the wave function and $\vec{r}$ and $\vec{k}$ the relative coordinate and momentum correspondingly. Assuming that the product $S_1 \cdot S_2$ is time independent, depends on $\vec{r}$ and has spherical symmetry, the correlation function can be approximated by [9]

$$C(k) \approx 1 + \int_0^\infty 4\pi r^2 dr S_{12}(r) \left[|\psi(k,r)|^2 - |j_0(kr)|^2\right], \tag{9}$$

with S_{12} the normalized pair source function (which we will be taken in the following form $S_{12}(r) = exp(-r^2/4R_{sf}^2)/(2\sqrt{\pi}R_{sf})^3$ [10]), ψ the scattering wave function and j_0 the order 0 spherical Bessel function. Since we are dealing with contributions coming from different channels, the formula must be modified [3]. Then, the properly constructed correlation formula is

$$C_i(k) = 1 + \sum_{j=1}^{10} \int_0^\infty 4\pi r^2 dr S_j(r) \omega_j \times \left[|\psi_{ji}(k,r)|^2 - \delta_{ji}|j_0(kr)|^2\right], \tag{10}$$

where i is the index of the channel considered, j an index that runs through all the channels and ω_j the conversion weights (they appear in order to properly account the contribution of each channel).

Regarding the wave function, ψ_{ji}, it is obtained considering the relations $|\psi\rangle = |\phi\rangle + GV|\psi\rangle$ and $V|\psi\rangle = T|\phi\rangle$, with the asymptotic form $\phi_l(kr) = j_l(kr)$ for arbitrary angular momentum [3]:

$$\psi_{ji,l}(k,r) = \delta_{ji} j_l(kr) + \int_0^{q_{max}} \frac{q^2 dq}{4\pi^2} \frac{2M_j}{E_{1j}E_{2j}} \frac{E_{1j}+E_{2j}}{s-(E_{1j}+E_{2j})^2+i\epsilon} j_l(qr) T_{ji;l}(q, \sqrt{s}). \tag{11}$$

Eq. (11) depends on angular momentum l, but our model is constructed considering only S-wave interactions, so we set $l = 0$. Regarding the T matrix, it has no dependence on q, then it can be taken out of the integral. Finally, the expression for the correlation function reads

$$C_i(k) = 1 + \sum_{j=1}^{10} \omega_j \int_0^\infty 4\pi r^2 dr S_j(r) \times \left[\left|\delta_{ji} j_0(kr) + \tilde{G}_j(\sqrt{s}) T_{ji}(\sqrt{s})\right|^2 - \delta_{ji}|j_0(kr)|^2\right], \tag{12}$$

with $\tilde{G}_j$ defined as

$$\tilde{G}_j(\sqrt{s}) = \int_0^{q_{max}} \frac{q^2 dq}{4\pi^2} \frac{2M_j}{E_{1j}E_{2j}} \frac{E_{1j}+E_{2j}}{s-(E_{1j}+E_{2j})^2+i\epsilon} j_0(qr). \tag{13}$$

Eq. (13) converges, in contrast to Eq. (7), and both real and imaginary parts contribute with a finite amount when $\epsilon \to 0$. Thus, no regularization is needed, but function below integral has a pole when

$$q = q_0 = \frac{\sqrt{(s-(M_j-m_j)^2)(s-(M_j+m_j)^2)}}{2\sqrt{s}}, \tag{14}$$

and it must be treated with some care, what will slow down the calculations. Obviously, a given channel j can contribute with a pole if it is open, i.e. if $\sqrt{s} \geq M_j + m_j$.

IV. RESULTS AND DISCUSSION

Two different numerical calculations for the correlation function

The pole that appears in the $\tilde{G}$ function, Eq. (13), has a crucial role in our numerical calculations. Using brute force method, i.e. directly calculating the integral of Eq. (13), in order to properly account for the contribution of this pole, the integral is divided in three intervals. One interval contains the pole and it should be small enough in order to accurately capture its contribution.

If we want to speed up the calculations, we introduce another method. The Eq. (13) shall be replaced by

$$\tilde{G}_j^{CR}(\sqrt{s}) = j_0(q_0 r) G_j^{CR}(\sqrt{s}, q_{max}) + \int_0^{q_{max}} \frac{q^2 dq}{4\pi^2} \frac{2M_j}{E_{1j}E_{2j}} \frac{E_{1j}+E_{2j}}{s-(E_{1j}+E_{2j})^2} \times (j_0(qr) - j_0(q_0 r)), \tag{15}$$

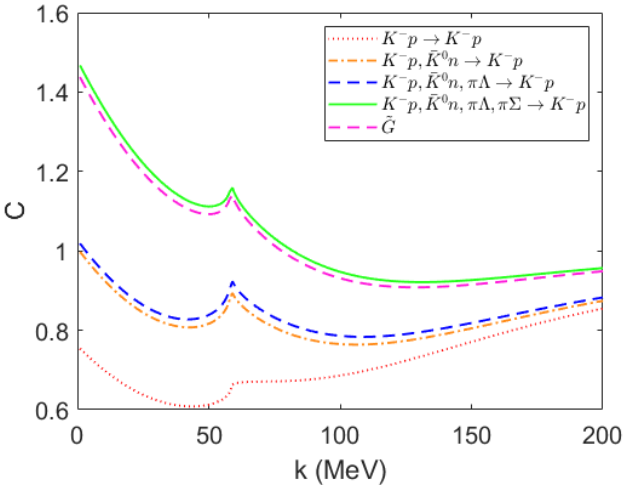

FIG. 2: K^-p correlations as a function of the center of mass momenta. The conversion weights have been set to 1 for all channels. In the same way, source functions radii are all equal to 1 fm. A upper limit of $q_{max} = 20\,GeV$ has been set for the integrals.

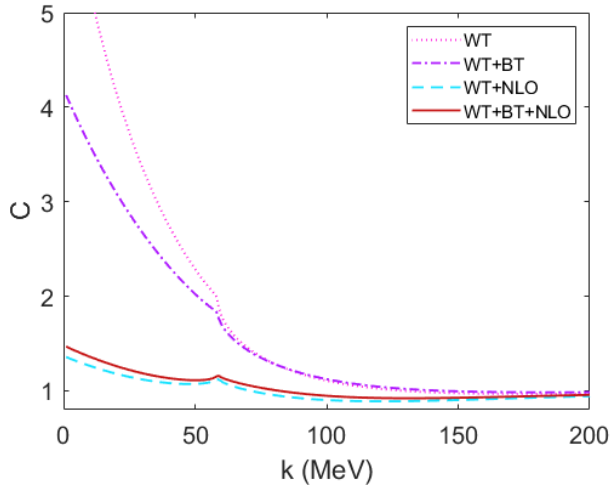

FIG. 3: Effects of the interaction potential term on the K^-p correlation function. The ω_j, R_{sf} and q_{max} are the same as those mentioned in Fig. 2.

where G^{CR} is the loop function calculated with a cutt off method mentioned above. What we gain is that the last term has no pole when q goes to q_0.

In Fig. 2, the results of the correlation function for the K^-p pair are shown using $\tilde{G}^{CR}$ (solid green line) and $\tilde{G}$ (dashed pink line) as a function of the center of mass momentum, k. In both cases Gauss quadrature method was employed for the integrals. Using $\tilde{G}^{CR}$ required only 100 points to reach convergence, while 5000 points were needed in the other case solely to compute the pole contribution and 5000 points more for the interval $[q_0, \text{inf}]$ (the interval $[0, q_0]$ was calculated using 5000 points too, but we could have taken 500 points instead).

The difference in the results between both methods is lower than 1.58% (value extracted by area comparison) and it is mainly due to the finite value of ϵ (we set $\epsilon = 10^{-3}\,MeV$). In order to get better results we should decrease the value of ϵ, but that would require a bigger number of points to achieve integral convergence and will consume many computational resources. From now on, all results presented will be derived from Eq. (15)

Channel and potential effects on the K^-p correlation function

Fig. 2 also shows the contribution of each channel to the K^-p correlation function. As can be seen, the effects of the $\pi\Lambda$ channel to the correlations is much smaller than that of $\bar{K}^0n$ and $\pi\Sigma$. The $\eta\Lambda$, $\eta\Sigma^0$ and $K\Xi$ channels do not contribute, because these are closed for $k \leq 200\,MeV$. Actually, $\bar{K}^0n$ channel does not contribute until $k \geq 58.57\,MeV$ and when it opens this generates a spike in the correlation function.

In Fig. 3 it is shown the contributions of the different potential terms used to compute the T matrix (see Eq. (2)). Note that using the WT and NLO interactions is enough to reproduce K^-p correlations with some accuracy; Born terms represent a $\sim 4.16\%$ correction.

Comparison with the ALICE Collaboration data of the K^-p correlation function

The results of the correlations of the K^-p channel experimentally obtained in Ref. [10] are shown in Fig. 4, 5 and 6 along with theoretical predictions. The conversion weights, ω_j, and the source functions radii were also collected from [10] for different centralities. The ω_j values have been obtained through a statistical model that takes into account the number of particle pairs produced after the collision. The used radii are visible in the figures too and following [10], r_{core} refers to the source function radius for the K^-p channel and $r^{\pi\Sigma}$ refers to the channels containing a π particle: $\pi\Sigma$ and $\pi\Lambda$.

Furthermore, in [10], scaling factors, α, were introduced to multiply the conversion weights of the $\bar{K}^0n$ and $\pi\Sigma$ channels in order to improve the agreement with experimental data (see Table I). The scaling factor for the $\pi\Lambda$ is set to 1 due to, again, its insignificant contribution to the correlations. In Fig. 4, 5 and 6 the scaling factors corrections are shown through the green solid lines, while the results without these corrections are shown with red dashed lines. It can be observed that introduction of α does improve the agreement with the data for our theoretical calculations as well. The model fits better to the data in the range $p = [45, 200]\,MeV$, but below $45\,MeV$, the model fails. We think that this deviation is due to the fact that Coulomb interaction between particles is not considered, which would lead to stronger correlations at low momenta [11].

To compare our model to the data more quantitatively χ^2 values are collected in Table I. These values are cal-

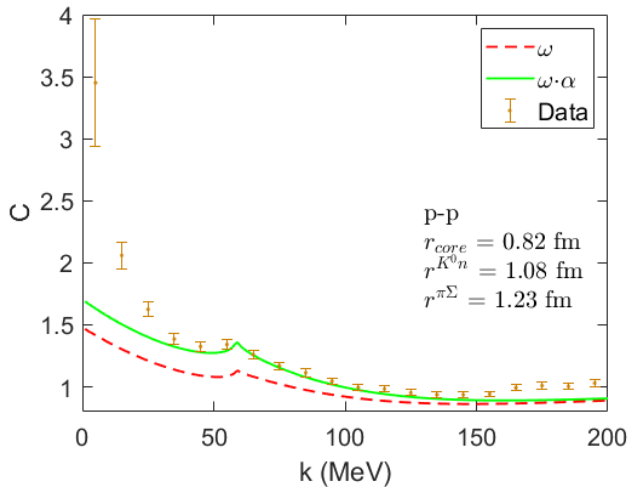

FIG. 4: Correlations of the K^-p channel collected from [10] when colliding $p-p$ particles at $\sqrt{s} = 13\,TeV$. Solid green and red lines are, respectively, the theoretical results and those calculations fixed using the scaling factors from Table I.

Collision	$\alpha_{\pi\Sigma}$	$\alpha_{\bar{K}^0 n}$
p-p	0.95286	2.22477
p-Pb 0-20%	1.0134	1.80101
p-Pb 20-40%	1.38952	1.90293
p-Pb 40-100%	1.42108	2.01129
Pb-Pb 60-70%	0.923531	1.46639
Pb-Pb 70-80%	0.886346	2.55656
Pb-Pb 80-90%	1.20194	2.04163

TABLE I: Scaling factors used in [10] to modify the conversion weights and fit the model to the data. The percentage values refer to interval centralities.

culated from the equation

$$\chi^2 = \frac{1}{N}\sum_i \frac{(C_i^{data} - C_i^{th})^2}{(\Delta C_i^{data})^2} \tag{16}$$

where C^{data} are data, ΔC^{data} are the corresponding errors and C^{th} are our theoretical results (using α); and N is the number of degrees of freedom, which is equal to the number of data points in our case (there are no free parameters in our calculations). Since our model does not fit the experimental data below $45 MeV$ the χ^2 values were computed for the interval $k = [45, 200]\,MeV$.

We can see that the best adjustment is obtained for $p-p$ and $p-Pb$ $40-100\%$ collisions. In general we obtain quite a fair agreement taking into account these are pure predictions for the model developed in Ref. [4], and the Coulomb interaction was ignored. Nevertheless, in all cases χ^2 is far away from unity which means that there is still place for improvement of the model, refitting the parameters to the new experimental data.

Collision	χ^2
p-p	6.47
p-Pb 0-20%	9.74
p-Pb 20-40%	10.83
p-Pb 40-100%	4.11
Pb-Pb 60-70%	15.17
Pb-Pb 70-80%	8.96
Pb-Pb 80-90%	10.05

TABLE II: χ^2 values obtained using correlation functions corrected by the scaling factors. The percentage values refer to interval centralities.

V. CONCLUSIONS

In this work we studied the K^-p correlation function using the ChUA of Ref [4], were the unitarization is implied in coupled channels. The results of our theoretical calculations have been contrasted to the experimental data from Ref. [10], and have shown reasonable agreement. It has been shown that $\bar{K}^0 n$ channel has an important role in the correlation function. Besides increasing the correlations, $\bar{K}^0 n$ also leads to the appearance of a spike at its opening threshold.

Interestingly enough, the adjustments made by the introduction of the scaling factors in Ref. [10] improve agreement of our model to data as well. However, the model fails to explain the experimental data and differs significantly for k values lower than $45\,MeV$. This deviation for lower momenta can be explained since we did not considered Coulomb interaction in all the calculus.

We also studied the partial contributions of the different terms forming the interaction potential of Ref. [4], Eq. (2). The functional form of the K^-p correlation function can be explained almost totally by the WT and NLO terms. In contrast, the Born terms only represent a little correction to the values in this case.

In order to calculate the correlation function, first we needed to calculate $\tilde{G}$ integral with a pole, Eq. (13). In this work we provide a comparison between two ways of calculating the correlation function for two different particles. Using Eq. (13) or Eq. (15) is indifferent, as both equations yield similar results. The difference between both expressions arises from the limited number of points that can be used to perform the integral near the pole and from the pole to infinity of Eq. (13).

Acknowledgments

I wish to thank Dr. Volodymyr Magas for all the valuable advices, supervision and guidance during all the project. Besides, I also would like to thank my parents for their eternal support.

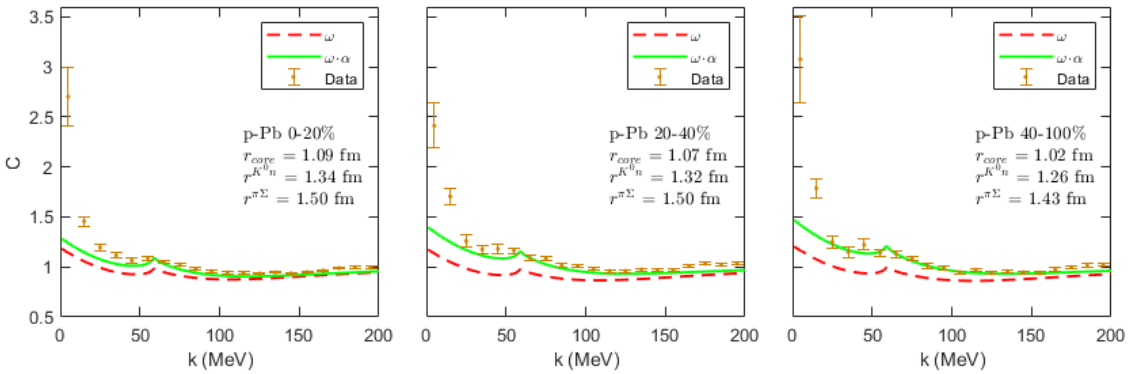

FIG. 5: Correlations of the K^-p channel collected from [10] when colliding $p-Pb$ particles at $\sqrt{s} = 5.02\,TeV$ in the $0-20\%$ (left), $20-40\%$ (middel) and $40-100\%$ centrality intervals. Solid green and red lines are, respectively, the theoretical results and those calculations fixed using the scaling factors from Table I.

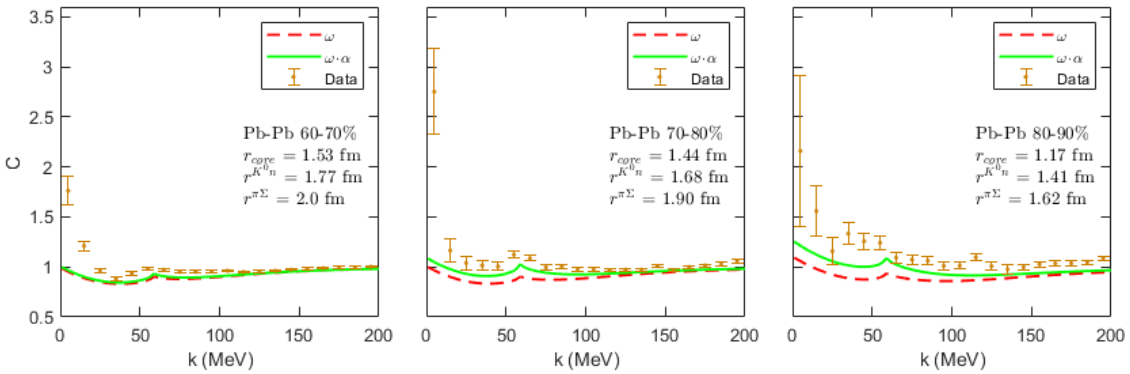

FIG. 6: Correlations of the K^-p channel collected from [10] when colliding $Pb-Pb$ particles at $\sqrt{s} = 5.02\,TeV$ in the $60-70\%$ (left), $70-80\%$ (middel) and $80-90\%$ centrality intervals. Solid green and red lines are, respectively, the theoretical results and those calculations fixed using the scaling factors from Table I.

[1] Verde, G. (2003). *Imaging two-particle correlations in nuclear reactions.*

[2] Pratt, S., Csörgő, T., & Zimányi, J. (1990). Detailed predictions for two-pion correlations in ultrarelativistic heavy-ion collisions. Physical Review C, 42(6), 2646.

[3] Haidenbauer, J. (2019). *Coupled-channel effects in hadron–hadron correlation functions.* Nuclear Physics A, 981, 1-16.

[4] Feijoo, A., Magas, V., & Ramos, A. (2019). *S = -1 meson-baryon interaction and the role of isospin filtering processes.* Physical Review C, 99(3), 035211.

[5] Hyodo, T., & Jido, D. (2012). *The nature of the Λ (1405) resonance in chiral dynamics. Progress in Particle and Nuclear Physics*, 67(1), 55-98.

[6] Feijoo A. (2012). *Reacción $\bar{K}N \to K\Xi$ en modelos quirales con canales acoplados hasta next-to-leading order.* Trabajo de Máster interuniversitario de Física nuclear, Universidad de Barcelona.

[7] Sakurai, J. J., & Commins, E. D. (1995). *Modern quantum mechanics, revised edition.*

[8] Oller, J. A., Oset, E., & Pelaez, J. R. (1999). *Meson-meson interactions in a nonperturbative chiral approach.* Physical Review D, 59(7), 074001.

[9] Ohnishi, A., Morita, K., Miyahara, K., & Hyodo, T. (2016). *Hadron–hadron correlation and interaction from heavy–ion collisions.* Nuclear Physics A, 954, 294-307.

[10] Acharya, S., Adamová, D., Adler, A. et al. (2023). *Constraining the $\bar{K}N$ coupled channel dynamics using femtoscopic correlations at the LHC.* Eur. Phys. J. C 83, 340.

[11] Borasoy, B., Nissler, R., & Weise, W. (2005). *Chiral dynamics of kaon-nucleon interactions, revisited.* The European Physical Journal A-Hadrons and Nuclei, 25, 79-96.